Journal of the European Ceramic Society 36 (2016) 791–796

Contents lists available at www.sciencedirect.com

Journal of the European Ceramic Society

journal homepage: www.elsevier.com/locate/jeurceramsoc

Bio-prototyping and thermoluminescence response of cellular rare earth ceramics

S.C. Santos*, C. Yamagata, L.L. Campos, S.R.H. Mello-Castanho

Instituto de Pesquisas Energeticas e Nucleares—IPEN, Av. Prof. Lineu Prestes 2242, Cidade Universitaria, Sao Paulo, Brazil

ARTICLE INFO

Article history:
Received 11 September 2015
Received in revised form 15 October 2015
Accepted 18 October 2015

Keywords:
Rare earths
Lanthanides
Bio-prototyping
Thermoluminescence
Ceramic processing

ABSTRACT

The use of renewable materials is essential toward green economy. Vegetable structures are abundant, exhibit complex hierarchically built shape and an architecture that is promising to form functional materials. In this work using a mixture of rare earth oxides, which contain around 57 wt% yttrium oxide, cellular ceramics by bio-prototyping from the vegetable sponge *Luffa cylindrica* were produced and the thermoluminescence response was evaluated. By colloidal processing aqueous suspensions with 25 vol% solids content, pH 10, 1 wt% defflocculant and 0.2 wt% binder exhibited shear thinning behavior and apparent viscosity suitable for replica method. By thermal treatment at 1600 °C for 2 h in air biomorphic rare earth ceramics with dense microstructure and reticulated architecture were produced.

1. Introduction

Rare earth elements (RE) have unique chemical and physical properties and therefore are very useful for high technological applications such as permanent magnets [1], batteries [2], thin films semiconductors [3], phosphors [4], petroleum catalysis [5], gas burners [6], radiation dosimeters [7], biological tracers [8] and diagnostic contrast [9]. Since no alternative materials that exhibit similar performance of RE have been found yet, UNEP (Global Environmental Alert Service) have done many alerts about the green economy vulnerability to rare earth minerals shortages [10]. In addition, any restriction in the production and supply of RE may have serious consequences for the world's transition to green energy supply, as well as may affect the global economy since the technologies are important in creating jobs, promoting economic growth, and fighting climate change.

From RE, yttrium oxide (Y_2O_3) also known as yttria has intrinsic chemical and physical properties as melting point around of 2400 °C, refractive index of 1.9, thermal and chemical stability [11,12]. Y_2O_3 is used for processing of advanced materials as sintering additive [13], catalysis [14], phosphors [15], ionic conductors [16], thin films [17], special alloys [18] and lasers [19]. Abe et al. [20] prepared yttrium doped europium (Y_2O_3:Eu^{3+}) nanoparticles by homogenous precipitation. The obtained nanoparticles exhibited strong and narrow red photo luminescent spectra, as well as promising biocompatibility. Li et al. [21] produced yttrium doped zinc oxide nanofibers (ZnO:Y_2O_3) by electrospinning method. The produced nanofibers exhibited uniform morphology, high specific surface area (40.2 $m^2 g^{-1}$) and gas sensing. Santos et al. [22] developed Y_2O_3 nettings with dense microstructure, reticulated structure and thermoluminescent response (λ = 550 nm and T = 150 °C) by colloidal processing and followed by replica from a nylon–cotton template.

Innovative actions toward green economy involves the controlled use of RE and smart process. In this context, colloidal processing leads the formation of reliable ceramic components whereby the ceramic suspension structure is controlled for a desired shape forming. This method is followed by thermal treatment for consolidation of the particles and formation of the final microstructure [23–25]. Moreover, the use of renewable materials such as wood [26], coral [27], cotton [28], and vegetable sponge [29] as templates to produce biomorphic functional ceramics leads also to green economy consolidation. Santos et al. [30], developed β-$Y_2Si_2O_7$ reticulated ceramics from biotemplating of the vegetable sponge gourd of *Luffa cylindrica*. The sponge architecture is promising for gas burner design because its reticulated structure can improve gas burning and light emission.

In this work a process to form cellular rare earth ceramics by bio-prototyping from *L. cylindrica* is presented. Apart from colloidal processing of rare earth oxides followed by replica method, cellular ceramics with reticulated structure and dense microstructure were produced.

* Corresponding author.
E-mail addresses: silas.cardoso@usp.br, silascs@ipen.br (S.C. Santos).

http://dx.doi.org/10.1016/j.jeurceramsoc.2015.10.024
0955-2219/

2. Experimental

RE_2O_3 powders (RE/wt% = Y/56.6; Dy/19.4; Er/6.5; Lu/4.1; Ho/3.1; Yb/2.0) with pycnometric density (ρ) of 6.03 g cm^{-3} and specific surface area (SSA) of 20.5.9 m^2 g^{-1} were produced through calcination of rare earth carbonate as reported in our previous work [6].

The thermoluminescence characterization of RE_2O_3 powders was performed with a TL reader (Risø TL/OSL-DA-20). The samples were evaluated at a heating rate of 10 °C s^{-1} up to 400 °C in nitrogen atmosphere.

The mean particle size (d_{50}) of RE_2O_3 was measured by means of Photon Correlation Spectroscopy (PCS, ZetaPALS Analyzer, Brookhaven Instruments). For PCS measurements an aqueous suspension with 0.01 vol% solids at pH 10, which is a good condition to disperse particles [30], was prepared. For dispersion of particles tetraethylammonium hydroxide (TMAH, Sigma–Aldrich) was used as defflocculant. The homogenization of ceramic suspensions was performed on a ball mill for 24 h.

RE_2O_3 aqueous suspensions with 25 vol% solids content were prepared at pH 10 from tetramethylammonium hydroxide (TMAH, Sigma–Aldrich), 1 wt% PAA (poly-acrylic ammonium acid, Sigma–Aldrich), 0.2 wt% CMC (carboxymethyl-cellulose, Sigma–Aldrich) based on the suspension weight. All suspensions were homogenized in a ball mill for 24 h, using alumina spheres ($Ø_{spheres}$ = 10 mm).

The flow behavior of RE_2O_3 suspensions was evaluated with a rheometer (Haake RS600, Thermo Scientific). The sensor system consisted of a double-cone rotor and a stationary plate (DC60/1°). The flow behavior of the suspensions was characterized in the control rate mode (CR) and compared with rheological models available in rheometer database (Haake Rheowin Data Manager v. 3.61.0.1). All measurements were evaluated at 25° by increasing the shear rate ($\dot{\gamma}$) from 0 to 1000 s^{-1} in 5 min, holding for 2 min at 1000 s^{-1} and returning to 0s^{-1} in 5 min. For each CR step 200 points were measured.

The vegetable sponge gourd (*L. cylindrica*, LCy) was used as a template once it exhibits a reticulated structure promising for gas burner technology. LCy samples were immersed in RE_2O_3 aqueous suspension for 30 min (optimized time) [31]. The impregnated samples were sintered in a vertical furnace (Lindberg/Blue M), where the thermal treatment conditions were based on thermal and gravimetric analysis results of LCy fibers (TGA/TDA, S60/38336 Setaram). The microstructure of the LCy fibers, impregnated samples and biomorphic replicas were evaluated with scanning electron microscopy (SEM, TM3000Hitachi and SEM, INCAx-act Oxford Instruments). The crystalline structure of the biomorphic RE_2O_3 replicas was evaluated by X-ray diffraction (XRD, Rigaku Multiflex), with scanning at 0.5° min^{-1}, from 10–80° (2Θ), Cu-Kα radiation.

3. Results and discussion

The mean particle size distribution of RE_2O_3 particles performed with PCS is shown in Fig. 1. As a result, RE_2O_3 particles exhibited a nanosized particle distribution with a mean diameter (d_{50}) of 722.6 nm, which is almost fifteen times higher than the theoretical diameter (d_{BET}) calculated from specific surface area (SSA) d_{BET} = 48.7 nm. This significant size difference was due to the shape factor (elongated particles, Fig. 1b) and the agglomerated state of particles, in which the agglomeration factor was very high around of 14.85. In addition, the difference between minor (d_{10}) and major (d_{90}) size distributions (Span) and the relative span were 294.1 nm and 0.41 respectfully.

Particle characteristics have a significant effect on ceramic processing from suspensions such as, packing density, size and shape of pore interstices, rheological behavior and drying, as well as microstructure formation [32]. Besides, particles which are in colloidal scale are ruled by surface forces being able to agglomerate easily [33]. As RE_2O_3 particles exhibit a shape factor far from spherical, nanosized particle distribution, high pycnometric density and agglomerated state the processing of ceramic suspensions have to be very effective in order to lead stable suspensions with suitable viscosity for replica method.

Fig. 2 shows the TL response of RE_2O_3 powders. From the result is observed that there was no formation of TL peaks from λ = 350 up to 750 nm. All emission of light took place on infrared range (λ = 750–4300 nm), where an intense peak was recorded at λ = 1000 nm and T = 400 °C. Considering that RE_2O_3 is constituted of a mixture of rare earth oxides (RE/wt% = Y/56.6; Dy/19.4; Er/6.5; Lu/4.1; Ho/3.1; Yb/2.0), the RE activator ions can interfere in luminescence behavior of each other and consequently in the TL response. In addition, particle characteristics have influence on luminescence performance, e.g. particle size, particle shape and surface roughness. Feofilov [34] reported that the time life of RE^{3+} ions tend to increase as a function of decreasing particle size. Bolshukhin [35] et al. showed that nanoparticles of $Sr_4Al_2O_3$:Eu^{3+} exhibits higher luminescence and luminous persistent.

The image by SEM of the LCy vegetable sponge used for formation of biomorphic ceramic components by replica method is shown in Fig. 3. The LCy template of pycnometric density ρ = 1.55 g cm−3 exhibits a reticulated structure (Fig. 3a), and fibers in random disposition like a web (Fig. 3b). The vegetable fibers presented a mean diameter of = 60 μm and a specific surface area SSA = 22.5 m^2 g^{-1}. In addition, vegetable fibers are composed of fibrils, which are joined together by a vegetal resin tissue (Fig. 3c).

The use of renewable materials is an important contribution for sustainable development. Nevertheless, it is usually necessary to do a previous treatment of the material before using [36–39]. The conditioning treatment depends on the type of vegetable sponge, type of soil, climate conditions and age of plant. For LCy template (Fig. 2d), the alkaline treatment with 2 wt% NaOH at 60 °C for 2 h was successful to remove surface substances such as cellulose and lignin. Besides, microchannels and scratches are visible on fibers surface (Fig. 2d—white arrows). In conclusion, the chemical treatment used in this work was suitable to clean fibers surface and to adequate the LCy template for impregnation method.

In Fig. 4 is shown the plot of flow curves of RE_2O_3 suspensions in CR mode up to 1000 s^{-1}. As described in our previous work [6], the stability conditions for RE_2O_3 suspensions are pH 10, 1 wt% PAA and 0.2 wt% CMC. Ceramic suspensions based on 25 vol% RE_2O_3 and prepared at these conditions exhibited shear thinning behavior, in which the apparent viscosity (η) decreases as the shear rate ($\dot{\gamma}$) increases. Extreme values of η are observed at $\dot{\gamma}$ <50 s^{-1} as a consequence of the ceramic suspension changed from static to flowing state. In addition, RE_2O_3 suspension exhibited η <100 mPa s from $\dot{\gamma}$ >200 mPa s, which indicates that ceramic particles were well dispersed. The rheological behavior of RE_2O_3 suspension in CR mode fitted to Cross model (η_0 = 14.27 mPa s; η_∞ = 23.11; $\dot{\gamma}$ = 2.397 s^{-1}; n = 0.2347). Besides, the ceramic suspension exhibited a thixotropy around of 4.394.10^{6}Pa.s^{-1} due to particle characteristics (size and shape), which lead to formation of agglomerates. Furthermore, the thixotropic behavior can be associated with extension of polymers chains, particles deformation, and break down of particle agglomerates formed by CMC binder.

Shear thinning suspensions are suitable for replica method. In this context, the suspension exhibits low viscosity as undergo a shearing and shows high viscosity in static condition. Hence, the ceramic suspension remains on the template surface during impregnation method. In Fig. 5 are shown images by SEM of LCy

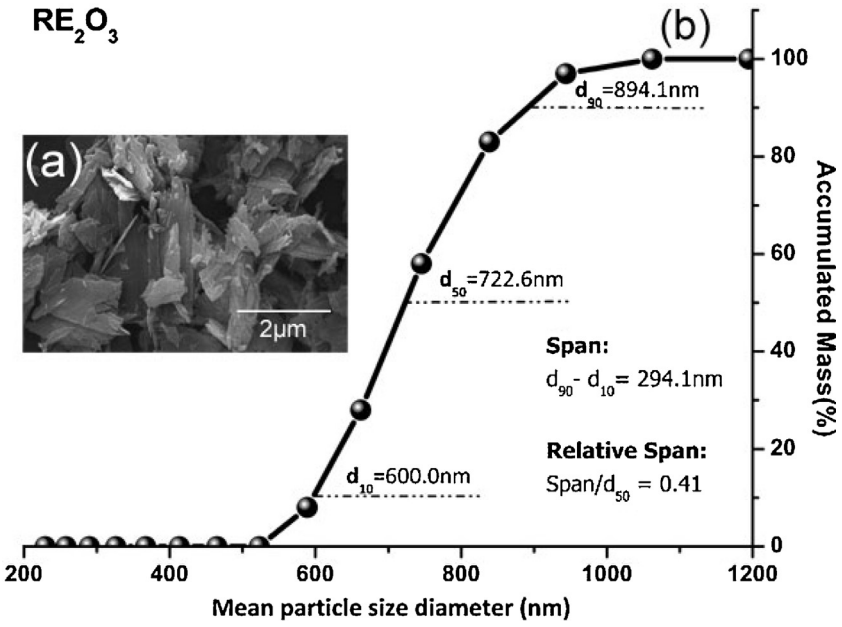

Fig. 1. Powder characterization of RE_2O_3 particles (a) SEM image of particles as flocks agglomerates;(b) mean particle size distribution by PCS.

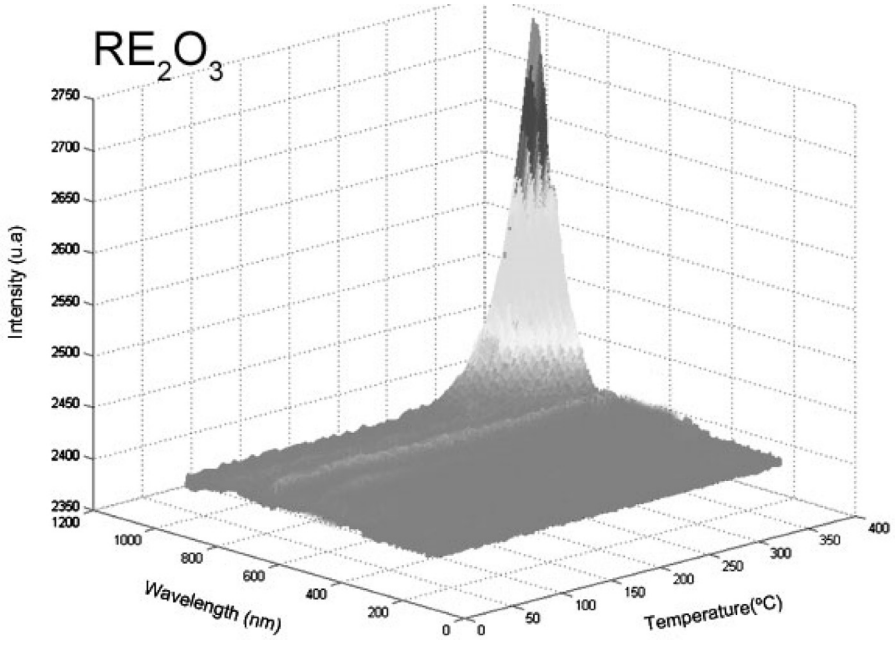

Fig. 2. Thermoluminescent response of R_2O_3 powders at heating rate of 2 °C s^{-1} until 400 °C in nitrogen atmosphere, in which no TL peaks were observed.

fibers after impregnation with RE_2O_3 suspension. It is clear that the ceramic suspension being well dispersed impregnated smoothly the LCy surface (Fig. 5a) like a painting. Furthermore, an internal part of the vegetable fiber was completely filled with the ceramic suspension, and even though RE_2O_3 particles morphology is far from spherical shape a homogeneous particle packing was formed. Therefore, the impregnation of LCy template with RE_2O_3 suspensions was successful [40].

Fig. 6a shows the RE_2O_3 burner prototype produced from biotemplating of the LCy vegetable sponge. Based on processing conditions, the RE_2O_3 burner exhibited loss weight around of 7%, pycnometric density of 6.03 g $cm^{-3}$and reticulated structure similar to LCy template (Fig. 6b). As shown in Fig. 6c and d ceramic fibers exhibit dense microstructure as well as heterogeneous distribution of grains size and shaped. In our prior study [6] the same microstructural characteristics was also observed for RE_2O_3 nettings sintered at 1600 °C for 1 h. In addition, from Fig. 6e and f it is observed that ceramic fibers exhibited transgranular fracture.

Fig. 7 shows XRD patterns of rare earth oxides, RE_2O_3, Dy_2O_3 and Y_2O_3. For RE_2O_3 all peaks were identified and indexed as Y_2O_3 C-type (PDF.70–603) and with the most intensity peak is around 29°. Possibly those diffraction peaks related to others rare earths oxides such as Er_2O_3, Lu_2O_3, Dy_2O_3, Ho_2O_3 and Yb_2O_3 were overwritten by those of Y_2O_3. Comparing RE_2O_3 to Dy_2O_3 pattern it is clear that the physical similarity of rare earths as the short distance between diffraction planes (d_{hkl}) could not be completely solved by XRD. In this context, Rietveld characterization should be useful to identify all rare earth diffraction planes.

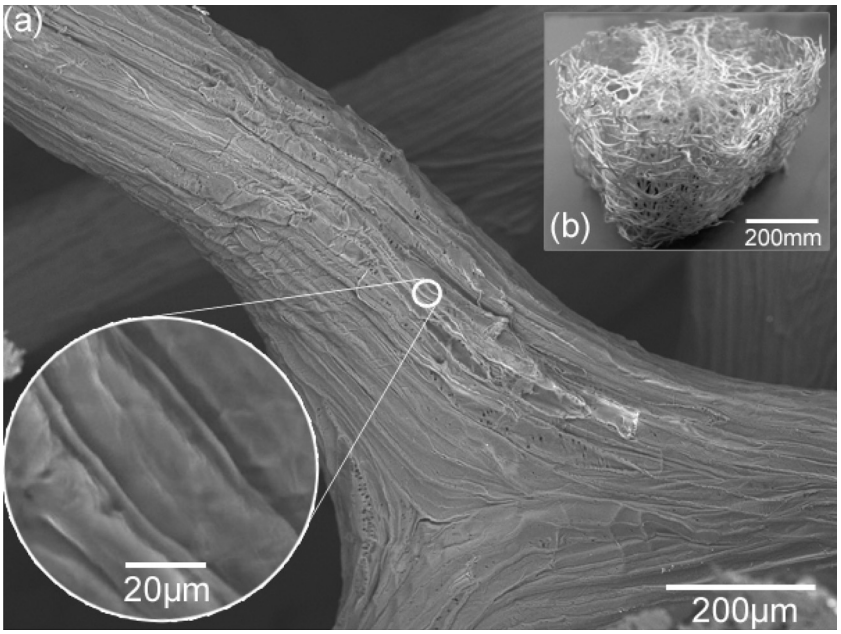

Fig. 3. SEM images of LCy (a) surface microstructure of fiber composed microchannels and (b) optical image of LCy template.

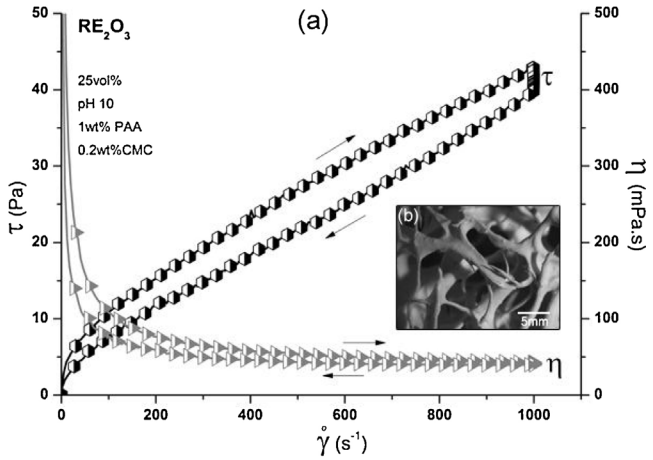

Fig. 4. (a) Flow curves of RE_2O_3 suspensions with 25 vol% solids content in CR mode up to 1000 s^{-1}; (b) optical image of LCy fibers impregnated with this suspension.

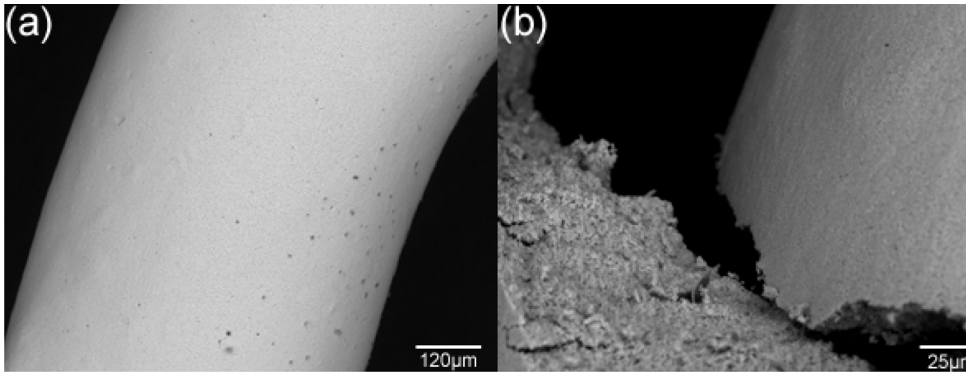

Fig. 5. SEM images of LCy impregnated samples, (a) smooth fiber surface and (b) internal surface of a fractured fiber showing ceramic particles deposited.

4. Conclusion

In the present work a biomorphic rare earth ceramic from biotemplating of the vegetable sponge gourd *L. cylindrica* and followed by colloidal processing of a mixture of rare earth oxides containing 56 wt% of yttrium oxide was produced. The rare earth powders exhibited no TL response. All emission of light fell on infrared and ultraviolet range due to the interference of different

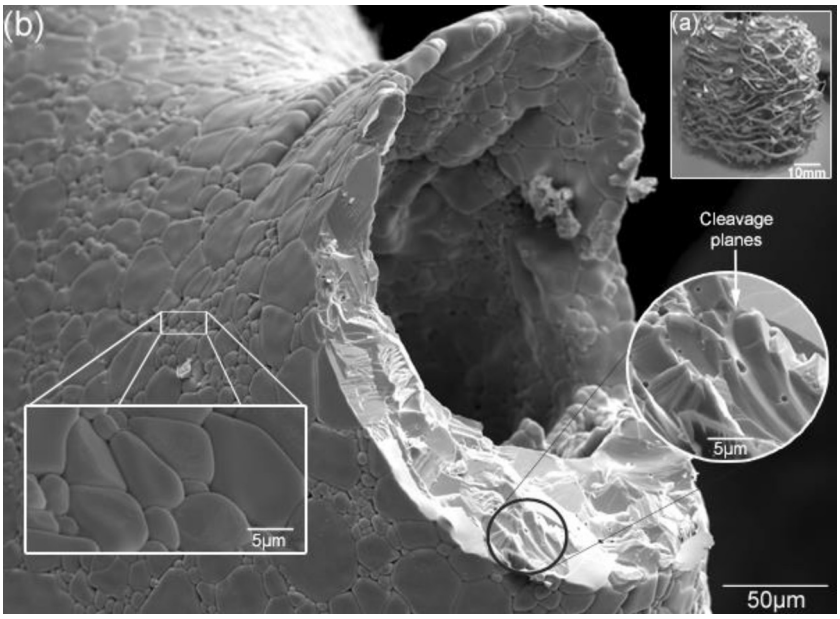

Fig. 6. (a) Biomorphic RE_2O_3 ceramic from biotemplating of LCy and sintered at 1600 °C for 2 h in air, (b) ceramic reticulated structure showing its hollow structure, transgranular fracture and cleavage planes.

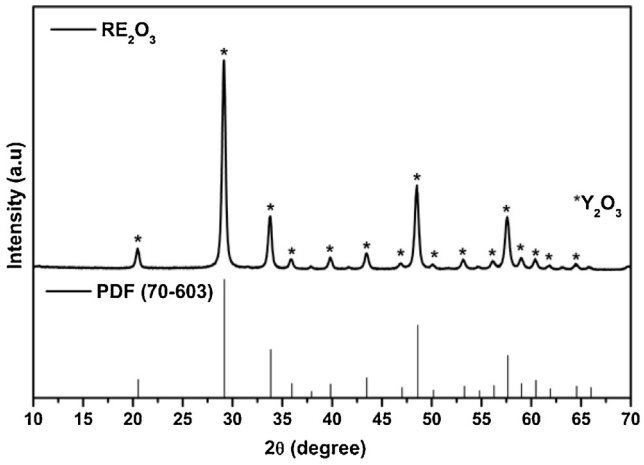

Fig. 7. XRD of biomorphic RE_2O_3 ceramics sintered at 1600 °C for 2 h. All peaks match Y_2O_3 standard (PDF. 70–623).

rare earth activator ions in luminescence response. Shear thinning suspensions with suitable apparent viscosity for replica method were prepared with 25 vol% solids content, pH 10, 1 wt% dispersant and 0.2 wt% binder. Using high temperature treatment at 1600 °C for 2 h in air, biomorphic rare earth ceramic with reticulated architecture, dense microstructure and pycnometric density of 6.03 g cm^{-3} was produced.

Acknowledgements

We authors are deeply grateful to Dr. Francisco Braga, Dr. Thomaz Augusto Restivo, Dr. Linda Caldas, Dr. Maira Tiemi Yoshizumi, MSc. Douglas Will Leite, and MSc. William Naville. In addition, grant #2014/23621-3, São Paulo Research Foundation (FAPESP); National Council for Scientific and Technological Development (CNPq); and Coordination for Improvement of High Degree People (CAPES).

References

[1] X.C. Wang, M.G. Zhu, W. Li, L.Y. Zheng, D.L. Zhao, X. Du, A. Du, The microstructure and magnetic properties of melt-spun CeFeB ribbons with varying ce content, Electron Mater. Lett. 11 (2015) 109–112.
[2] R. Lacal-Arantegui, Materials use in electricity generators in wind turbines—state-of-the-art and future specifications, J. Clean Prod. 87 (2015) 275–283.
[3] R. Cobas, S. Munoz-Perez, S. Cadogan, M.C. Ridgway, X. Obradors, Surface charge reversal method for high-resolution inkjet printing of functional water-based inks, Adv. Funct. Mater. 25 (2015) 768–775.
[4] Y.H. Wang, G. Zhu, S.Y. Xin, Q. Wang, Y.Y. Li, Q.S. Wu, C. Wang, X.C. Wang, X. Ding, Recent development in rare earth doped phosphors for white light emitting diodes, J. Rare Earth 33 (2015) 1–12.
[5] Y. Saka, N. Chiyoda, K. Watanabe, Effect of mono aluminum phosphate as new matrix component on cracking performance of FCC catalyst, J. Jpn. Petrol. Inst. 58 (2015) 40–45.
[6] S.C. Santos, S. Yamagata, S. Mello Castanho, Lighting by biogas burners: perspectives on development in Brazil, J. Mater. Sci. Appl. (2014).
[7] L.C. Matsushima, G.R. Veneziani, R.K. Sakuraba, J.C. da Cruz, L.L. Campos, Dosimetric study of thermoluminescent detectors in clinical photon beams using liquid water and PMMA phantoms, Appl. Radiat. Isot. 70 (2012) 1363–1366.
[8] B. Danko, Z. Samczynski, R. Dybczynski, Analytical scheme for group separation of the lanthanides from biological materials before their determination by neutron activation analysis, Chem. Anal. (Warsaw) 51 (2006) 527–539.
[9] E. Zobeiri, A.B. Moghaddam, F. Gudarzy, H. Mohammadi, S. Mozaffari, Y. Ganjkhanlou, Modified Eu-doped Y2O3 nanoparticles as turn-off luminescent probes for the sensitive detection of pyridoxine, Luminescence 30 (2015) 290–295.
[10] U.N.E. Programme, Green Economy Vulnerable to Rare Earth Minerals Shortages, UNEP, 2011, 2015.

[11] A. Abrão, Química e tecnologia das terras raras, CETEM/CNPq, Rio de Janeiro, 1994.
[12] T. Moeller, The Chemistry of the Lanthanides, Pergamon Press, 1975, 2015.
[13] M. Marina, M.Z.M. Zamzuri, M.N. Derman, M.A. Selamat, Z. Nooraizedfiza, Comparison study in consolidation of yttria reinforced iron–chromium composites using conventional and microwave sintering technique, Adv. Mater. Eng. Technol. (II) 594–595 (2014) 832–836.
[14] F. Hayashi, M. Tanaka, D.M. Lin, M. Iwamoto, Surface structure of yttrium-modified ceria catalysts and reaction pathways from ethanol to propene, J. Catal. 316 (2014) 112–120.
[15] X.M. Han, X. Feng, X.W. Qi, X.Q. Wang, M.Y. Li, The photoluminescent properties of Y_2O_3:Bi^{3+}, Eu^{3+} Dy^{3+} phosphors for white-light-emitting diodes, J. Nanosci. Nanotechnol. 14 (2014) 3387–3390.
[16] A. Jyotsana, G.S. Maurya, A.K. Srivastava, A.K. Rai, B.K. Ghosh, Synthesis and electrical properties of Y2O3: Dy3+ & Eu3+ nanoparticles, Appl. Phys. A-Mater. 117 (2014) 1269–1274.
[17] T. Mongstad, A. Thogersen, A. Subrahmanyam, S. Karazhanov, The electronic state of thin films of yttrium, yttrium hydrides and yttrium oxide, Sol. Energ. Mat. Sol. C 128 (2014) 270–274.
[18] M.A. Auger, V. de Castro, T. Leguey, J. Tarcisio-Costa, M.A. Monge, A. Munoz, R. Pareja, Effect of yttrium addition on the microstructure and mechanical properties of ODS RAF steels, J. Nucl. Mater. 455 (2014) 600–604.
[19] J. Hostasa, J. Matejicek, B. Nait-Ali, D.S. Smith, W. Pabst, L. Esposito, Thermal properties of transparent Yb-Doped YAG ceramics at elevated temperatures, J. Am. Ceram. Soc. 97 (2014) 2602–2606.
[20] S. Abe, Y. Hamba, A. Hyono, S. Yamagata, M. Uo, J. Iida, T. Kiba, A. Murayama, T. Akasaka, F. Watari, Preparation and biocompatibilities of luminescent europium-doped yttria and titania nanoparticles, J. Ceram. Soc. Jpn. 122 (2014) 216–221.
[21] X.B. Li, Q.Q. Zhang, S.Y. Ma, G.X. Wan, F.M. Li, X.L. Xu, Microstructure optimization and gas sensing improvement of ZnO spherical structure through yttrium doping, Sens. Actuators B-Chem. 195 (2014) 526–533.
[22] S.C. Santos, W. Acchar, C. Yamagata, S. Mello-Castanho, Yttria nettings by colloidal processing, J. Eur. Ceram. Soc. 34 (2014) 2509–2517.
[23] J.A. Lewis, Colloidal processing of ceramics, J. Am. Ceram. Soc. 83 (2000) 2341–2359.
[24] F.F. Lange, Colloidal processing of powder for reliable ceramics, Curr. Opin. Solid State Mater. 3 (1998) 496–500.
[25] R. Moreno, Reología de suspensiones cerámicas, Consejo Superior de Investigaciones Científicas, Madrid, 2005.
[26] S.K. Tang, X.L. Cui, L. Gu, H. Zhou, X.W. Zhang, A novel co-templating method for hierarchical mesoporous alumina monoliths replica, Funct. Mater. Lett. 6 (2013).
[27] H.X. Niu, Q. Yang, K.B. Tang, Y. Yie, Self-assembly of porous MgO nanoparticles into coral-like microcrystals, Scr. Mater. 54 (2006) 1791–1796.
[28] T.X. Fan, B.H. Sun, J.J. Gu, D. Zhang, Biomorphic Al_2O_3 fibers synthesized using cotton as bio-templates, Scr. Mater. 53 (2005) 893–897.
[29] S.A. Silva, D.D. Brunelli, F.C.L. Melo, G.P. Thim, Preparation of a reticulated ceramic using vegetal sponge as templating, Ceram. Int. 35 (2009) 1575–1579.
[30] S.C. Santos, C. Yamagata, A.C. Silva, L.F.G. Setz, S.R.H. Mello-Castanho, Yttrium disilicate micro-cellular architecture from biotemplating of *Luffa cylindrica*, J. Ceram. Sci. Technol. 5 (2014) 203–208.
[31] S.C. Santos, C. Yamagata, W. Acchar, S.R.H.M. Castanho, Yttria nettings by replica processing, Mater. Sci. Forum 798 (2014) 3.
[32] J. Reed, Principles of Ceramics Processing, 2nd ed., John Wiley & Sons, New York, 1995.
[33] N.V. Derjaguin, V.M. Churaev, The Derjaguin–Landau–Verwey–Overbeek (DLVO) Theory of Stability of Lyophobic Colloids, Surface Forces, Springer, US, 1987, pp. 293–310.
[34] S.P. Feofilov, Spectroscopy of dielectric nanocrystals doped by rare-earth and transition-metal ions, Phys. Solid State+ 44 (2002) 1407–1414.
[35] N.P. Bolshukhin, V.N. Soshchin, A.D. Lichmanova, Effect of dispersion on optical?physical parameters of luminescence, Proceedings of the International Conference on Nanotechnology (2004) 202–206.
[36] V.O.A. Tanobe, T.H.D. Sydenstricker, M. Munaro, S.C. Amico, A comprehensive characterization of chemically treated Brazilian sponge-gourds (*Luffa cylindrica*) (vol. 24, p. 474, 2005), Polym. Test. 29 (2010) 288–289.
[37] V.O.A. Tanobe, T.H.D. Sydenstricker, M. Munaro, S.C. Amico, A comprehensive characterization of chemically treated brazilian sponge-gourds (*Luffa cylindrica*), Polym. Test. 24 (2005) 474–482.
[38] C.A. Boynard, S.N. Monteiro, J.R.M. d'Almeida, Aspects of alkali treatment of sponge gourd (*Luffa cylindrica*) fibers on the flexural properties of polyester matrix composites, J. Appl. Polym. Sci. 87 (2003) 1927–1932.
[39] E. Sjöström, Wood Chemistry, in: Fundamentals and Applications, Academic Press, 1993.
[40] H. Zou, S.D. Li, X.B. Wu, M.J. M.cDonald, Y. Yang, Spray-drying synthesis of pure Na_2CoPO_4F as cathode material for sodium ion batteries, Ecs. Electrochem. Lett. 4 (2015) A53–A55.